UNIVERSIDAD CARLOS III DE MADRID
ESCUELA POLITECNICA SUPERIOR

DEPARTMENT OF BIOENGINEERING AND AEROSPACE ENGINEERING

BACHELOR THESIS:

Experimental investigation of non linear flame dynamics.

Author: David Calvo Ferreira
Supervised by: Yacine Babou

Acknowledgements

Looking back throughout these months of work, I realized that the fulfillment of this project would have been impossible without the collaboration and guidance of professors and collaborators, or without the support and help of the closest people. Because of this, I would like to thank and dedicate this work to the following people:

In the first place, to my thesis' supervisor, Yacine Babou, for his constant presence throughout the project and his willingness at the time of solving my doubts and helping me in my setbacks.

In addition, I want to mention and give my gratitude to Mario Sánchez Sánz and Fernando Veiga López, whose help and collaboration was fundamental for the realization of the experimental part of this thesis.

I equally mention the members of this jury, as well as the professors of the university and my classmates, with whom I have learned and grown up during these years.

Finally, my last words go to my most unconditional support: my parents, Alcinda and José Luis, for their patience and sacrifice in the hardest moments of this stage; And to my girlfriend, Natalia, for her continuous support and encouragement in this project as well as in any situation in which I have needed it.

In general, to all the people that have made this possible, thank you.

Abstract

The goal of the project is to develop a method to characterize flame instability by means of image processing. To apply this process it is necessary the obtaining of data coming from experiments.

The transformation for Cartesian coordinates to channel-fitted curvilinear coordinates is a very important tool, since it allows to improve the representation of the peaks that appears on the flame, making simpler their identification. Also, this conversion process requires the creation of baselines from which it will take the reference view.

All this tool were performed using the software tool ®MatLab, creating a code that will give the results expected.

Before applying the analysis it was necessary to realize an experiment, executed in the laboratories inside Universidad Carlos III de Madrid, described by flame propagation inside a configuration of the Hele-Shaw cell, while the process is recorded using a High Speed camera storing the output inside a computer.

The objective of the code created is to be a tool that will help and simplify the identification of the instabilities that arise in the flame.

Contents

List of Figures

List of Tables

1 Introduction

Combustion instabilities arises various coupling phenomena eg. combustion-acoustic interactions. Dangerous pressure and heat release rate oscillations are a possible result in practical combustion systems, which mainly affect engines eg. Rocket motors or jet and gas-turbine engines [1]. Due to their threatening nature, the study of swirling flames, that can be originated in the previous engines, is of great importance in the aircraft propulsion industry and in the electricity production power plants: an adequate design and consideration of these singularities is fundamental.

The origination of oscillations due to the flame instabilities can affect the structures causing mechanical and thermal loading, and a significantly increment of the emission of pollutant gas in combustion processes. Therefore, flame instabilities have a negative impact on the system's efficiency, safe operating range, and life-span [1]. Deflagration-to-Detonation Transition (DDT), which is the appearance of inflammable mixtures of gas and air that appear when a deflagration type of combustion suddenly transits to a detonation type of explosion, can be caused by multidimensional flame instabilities [2]. On the other hand, one-dimensional flame instabilities provoke in the fire-chambers vibratory combustions that lead to rapid variations of pressure and velocity in space and time [3].

Mainly, the analysis of the combustion instabilities is performed in linear analysis, however most of the experiments prove that the recognition of the instabilities is more adequate in the non-linear regime [4].

The principal non-linear element of the system is identified as the flame of the combustion, and its response to perturbations is represented as a function of the gain and phase which are directly dependent to the input's amplitude [4].

Therefore, in this situation the fundamental frequency is implied to be predominant and higher frequencies, that originate in the non-linear element, are lost and filtered out by the rest of the system's components [4].

1.1 First experiments on flame instabilities

Planar flame sheets tend to automatically create cellular structures, as they are highly influenced by perturbations and unstable. The gas expansion originated by heat release in a wrinkled premixed flame arises the flow line in the front

towards the flame's normal direction. which was first discovered by Darrieus in 1938 [5]. The previous phenomenon creates a divergence in the flow and gradients of velocity that increase the wrinkling of the flame as portrayed in figure 1 [6].

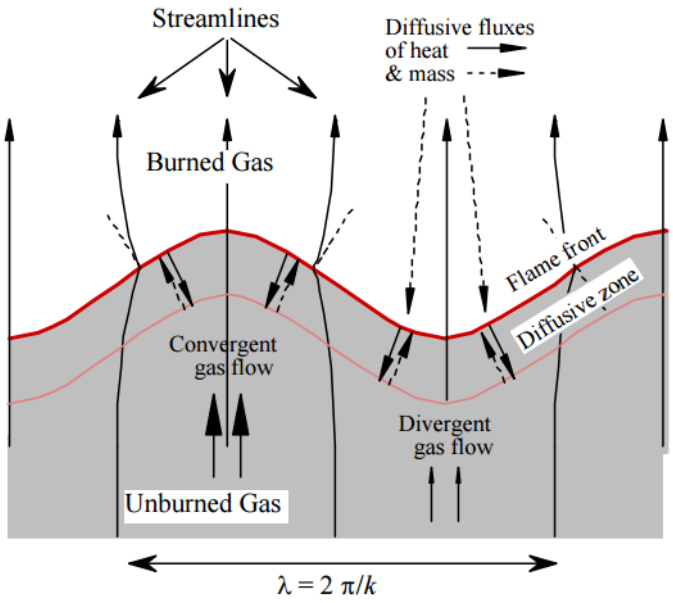

Figure 1: Structure of a wrinkled flame front showing the hydrodynamic streamlines and the diffusive fluxes of heat and mass. Taken from [6].

In 1994 Landau independently defined this unconditional hydrodynamic instability. It is based on considering the flame as a thin interface between unburned and burned gases which allows to build a relation between the instability's growth rate with the wavenumber perturbation and the expansion rate of the gas [6].

1.2 Experiment

In the frame of this context, the ambition of the project carried out at the Bioengineering and Aerospace Engineering department is to provide a proper method to extract critical information about the development of instabilities of premixed flame in a Hele-Shaw cell geometric configuration. To accomplish this aim, a method of image processing is developed to track the variation of the flame length and the formation of cells. The method is applied to Hele-Shaw cell data. These

experiments were performed at Universidad Carlos III de Madrid as explained in Section 3.

The code is developed using ®MatLab. Using this code the images are read and processed. Once the set of images is previously treated to allow ®MatLab to work with them, the principal way to represent the instabilities is to figure out a method to extract the surface of the flame where these disequilibrium appear.

Finally, the emergence of instabilities is characterized by the peaks that emerge on the flame and the most interesting part to be taken into account is how these perturbations grow through time.

In Appendix A, the socio-economic environment is explained.

1.3 Regulatory framework

As the experiment analyzed is based on the combustion of an inflammable gas, in this case propane, some security measures must be applied [7]:

- Wearing adequate laboratory clothes (including anti-ignition gloves and glasses).
- Controlling the pressure and the mass flow of the gas from the source.
- Performing the experiment and storing the propane in an isolated location away from heat and light.
- Forbidding ignitable devices or materials.
- Preparing an emergency plan for fire extinction and disposing of extinguisher.
- To limit the time exposed to the gas and to examine the ventilation devices to check that they fulfill the environmental requirements.

In this project the software ®MatLab were employed to perform the image processing of the data, since it is a commercial software its license needs to be purchased.

As it is said in ®MatLab web page [8]: "Student software is for use by students on student-owned hardware to meet course requirements and perform academic research at degree-granting institutions only. It is not available for government, commercial, or other organizational use".

2 Flame Instability

As it is explained in Section 1, in the combustion studies is of highly relevance to consider the propagation of premixed flames in narrow channels, tubes, gaps and slot; eg. in the study of hydrocarbon emissions originated in partial burning or flame quenching in internal combustion engines [9].

The Hele-Shaw cell, is a related but different configuration. During this experiment the Hele-Shaw cell is applied and explained in detail in Section 3.

2.1 Types of instabilities

There are two main modes of instabilities in premised combustion: the hydrodynamic and the diffusive-thermal instability [10]. But for this case with a Hele-Shaw cell configuration it may appear other types of flame instabilities, as explained by Daniel Fernández-Galisteo, Vadim N. Kurdyumov and Paul D. Ronney [9]:

- "The Darrieus-Landau (DL) or hydrodynamic instability due to the density across the flame front. It occurs for any propagating front in which the density of the products is less than that of the reactants, which is the case for essentially all flames."
- "The Rayleigh-Taylor (RT) instability due to buoyant convection. Its effects are destabilizing for upward-propagating flames because in this configuration the lower-density fluid lies underneath the higher-density fluid, whereas for downward-propagating flames, its effects are stabilizing."
- "The Saffman-Taylor (ST) instability due to the viscosity change across the flame front. (ST) effects are destabilizing when a less-viscous fluid displaces a more-viscous fluid, which is the case for essentially all flames since the viscosity of gases increases with temperature and thus the burned products have higher viscosity than the unburned reactants."
- "The diffusive-thermal (DT) instability due to the unequal values of thermal vs. molecular diffusion coefficients as characterized by the Lewis numbers (Le) of the reactants. (DT) effects are destabilizing for (Le) less than a critical value near unity and stabilizing for larger (Le)."

These instabilities are the cause of an effect of wrinkle on the flame's front and the modification of its overall propagation rate even when the laminar state remains in the gas flow. "Joulin and Sivashinsky modeled the flame front as an infinitely thin discontinuity with specified local normal propagation speed and derived a dispersion relation expressing the growth rate of the instability in terms of the density and viscosity differences across the front and the buoyancy effect" [9].

2.2 Flame Stretch

The dependence of the flame speed on flow conditions is highly relevant in the studies of flame instabilities [11].

> "Flame stretch is defined as the fractional are change of a Lagrangian surface element of the flame surface .it is a kinematics concept" [11].

$$\mathbb{K} = \frac{1}{A}\frac{dA}{dt} \tag{1}$$

2.2.1 General flame surface [11]

$$\mathbb{K} = \underbrace{S_L \mathscr{K}}_{(a)} \overbrace{\underbrace{-(v \cdot n)\mathscr{K}}_{(b)} + \underbrace{\nabla_\tau \cdot v_\tau}_{(c)}}^{overall\ strain\ K_S} \tag{2}$$

(a) "the normal propagating motion can expand or contract the flame depending on the sign of the curvature."

(b) "normal straining caused by v_n can contract or expand the flame depending on the sign of the curvature."

(c) "tangential straining represented by the divergence of the tangential velocity vector, can have a compressing or expanding effect."

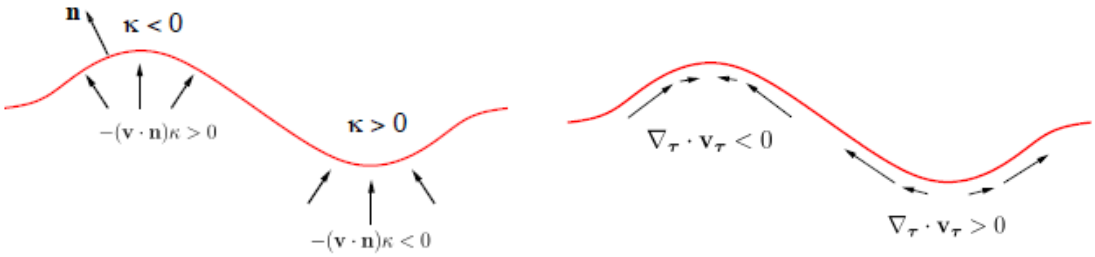

(a) Normal straining (b) Tangential straining

Figure 2: Straining's types. Taken from [11]

3 Experimental Setup

The experiment was performed at the laboratories at Universidad Carlos III de Madrid by professors and partners from the Thermal and Fluids Engineering department.

For this investigation a practical example of the Hele-Shaw cell was reproduced. It is a configuration employed to study flame instability as shown in figure 3.

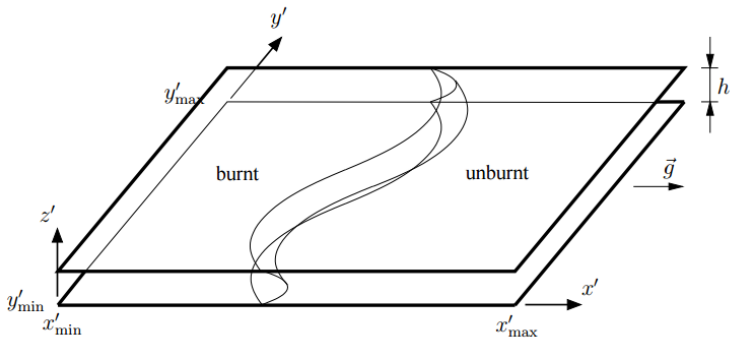

Figure 3: Hele-Shaw cell. Taken from [9]

This type of configuration consists of a region with a small and uniform depth in the z-dimension, while the dimensions in the x-direction and y-direction are much larger. These devices have been fabricated by means of two flat plates close together [12].

The complete setup, built by Fernando Veiga López, is composed by:

- A reproduction of the Hele-Shaw cell made of two methacrylate plates with a separation of 1 cm between them, these plates are 1 meter long and 0.5 meters wide. The complete device is sustained by an aluminum support.
- A Memrecam HX-3 High Speed Camera shown in figure 4.
- Nac Image Technology software installed in the computer to control the camera and store the files.
- A glow plug used to ignite the flame.

Figure 4: Memrecam HX-3 High Speed Camera. Taken from [13].

The setup works by means of a glow plug that is a pencil-shaped piece of metal with a heating element at the tip, this heating element, when electrified, heats due to its electrical resistance and it ignites the gas after its injection inside the Hele-Shaw cell [14], the gas used was propane with a fuel–air equivalence ratio (ϕ) of 1. When it starts to burn, the flame's propagation is recorded employing the high speed camera.

Before recording, the contrast of the camera must be increased to make the flame visible, also the frame rate is set. Once the main parameters are established, the flame is captured and stored in the computer by means of Nac's software that controls the camera. The video is saved as a set of images with .tiff format, which are the ones analyzed in Section 5. The flame propagation of the set of images studied was recorded at 4000 frames per second (fps).

4 Image processing approach

In this section, it is presented the approach adopted to extract meaningful information about flame instability from the digital images obtained during the experimental measurement described in Section 3. The following figure 5 shows the set of images that will be analyzed.

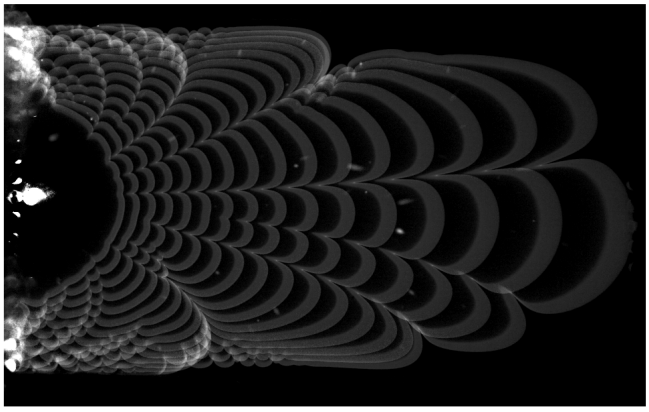

Figure 5: Sequence of images.

In order to perform a successful method to process the images, it was necessary to take into account two previous aspects:

- Learning about transformation of coordinates; in this case Cartesian to channel fitted curvilinear coordinates. This will be used to easily achieve a method to count the peaks related with the instabilities of the flames.
- To develop the best method of processing images; it is useful to create an assessment with a prescribed shape that is simpler than the real data.

4.1 Transformation

The transformation from Cartesian to channel fitted coordinates is a very important aspect for this experiment: it allows to change the reference frame making simpler to recognize the instabilities. With the implementation of this conversion, it is possible to count the peaks that are related to the instabilities that are wished

to be studied.

This transformation was developed by means of some functions implemented in ®MatLab. These functions transform Cartesian to channel fitted coordinates using a given curve which will be the baseline of the points or curves that are required to be transformed.

A representation of both coordinate systems is displayed in figure 6:

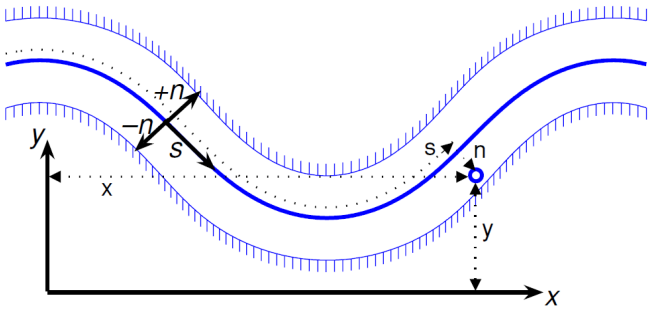

Figure 6: Cartesian (x,y) and channel-centered curvilinear (s,n) coordinate systems. Taken from [15].

The principal function is *xy2sn*. This function takes the coordinates of the profile to be analyzed together with the coordinates of the baseline obtained through the steps that are explained in Section 4.2. It is based in the use of a spline interpolation procedure to give the coordinates of the curve analyzed taking each point of the baseline as the reference ones, as it was explained by Carl J. Legleiter and Phaedon C. Kyriakidis [15]. As it can be noticed in the flowchart represented in figure 7.

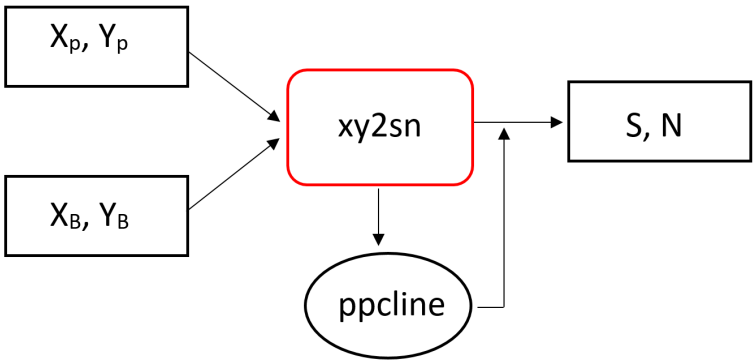

Figure 7: Flowchart explaining the transformation.

Where:

- X_P and Y_P are the x and y Cartesian coordinates of the profile of the flame.
- X_B and Y_B are the x and y Cartesian coordinates of the baseline.
- S and N are the channel fitted coordinates obtained from the transformation.
- *ppcline* is the function that makes splines of baseline parametrized to baseline length.

4.2 Applying method using a prescribed shape

In order to develop a proper analysis, an example very similar to the profile observed in figure 5 is created. This process will help to identify the different improvements that must be performed to the method, by using synthetic profiles to some extent that represents a real flame shape, until achieving the more adequate baseline geometry required to fulfill the analysis.

The process begins considering academic examples that have the shape of a sinusoidal plot combined with a circle and ellipse giving by equations 3 and 4 respectively. Each of these combinations are represented in figure 8 and figure 9.

$$\begin{aligned} x &= (R + A \cdot \sin(n \cdot t)) \cdot \cos(t) + X_c \\ y &= (R + A \cdot \sin(n \cdot t)) \cdot \sin(t) + Y_c \end{aligned} \tag{3}$$

$$\begin{aligned} x &= (X_r + A \cdot \sin(n \cdot t)) \cdot \cos(t) + X_c \\ y &= (Y_r + A \cdot \sin(n \cdot t)) \cdot \sin(t) + Y_c \end{aligned} \tag{4}$$

Where:

- x and y are the coordinates position of the curve respectively.
- R is the radius of the circle.
- X_r and Y_r are the two radius of the ellipse respectively.
- t is a set of values from 0 to 2π radians.
- A is the amplitude of the embedded sinus.
- n is the number of sinus of the profile.
- X_c and Y_c are the center positions where the curve is set.

All of these parameters were treated as non dimensional and have no units, since they are academic examples.

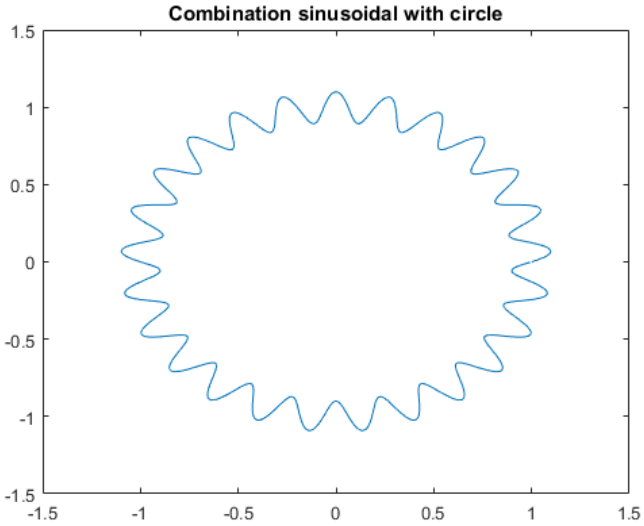

Figure 8: Combination of sinusoidal with circle.

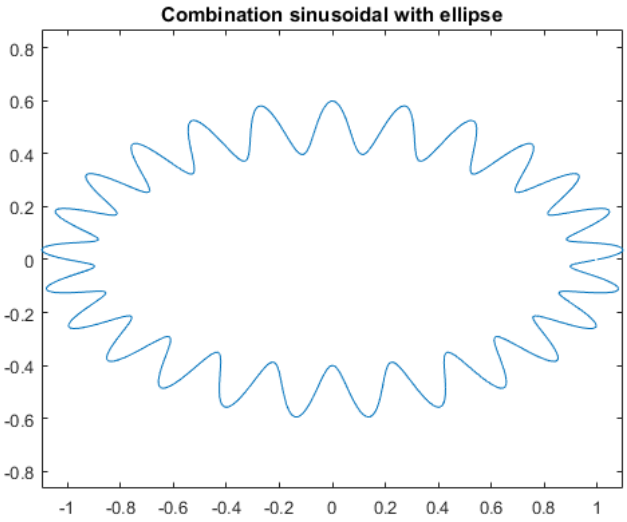

Figure 9: Combination of sinusoidal with ellipse.

For each one of this curves, three different baselines were created:

- A circle given by equation 5:

$$\begin{aligned} x &= R \cdot \cos(t) + X_c \\ y &= R \cdot \sin(t) + Y_c \end{aligned} \tag{5}$$

- An ellipse given by equation 6:

$$\begin{aligned} x &= X_r \cdot \cos(t) + X_c \\ y &= Y_r \cdot \sin(t) + Y_c \end{aligned} \tag{6}$$

Once the baselines are obtained, the transformation from Cartesian to channel fitted curvilinear coordinates is accomplished applying the functions and procedure explained in Section 4.1. This conversion is performed for each of the combinations of the prescribed curves with its baselines. The representation of the combination with its transformed is displayed in figure 10, figure 11, figure 12 and figure 13. The red line that appears in the transformation figures 10b, 11b, 12b and 13b

represents the baseline converted and its profile's length.

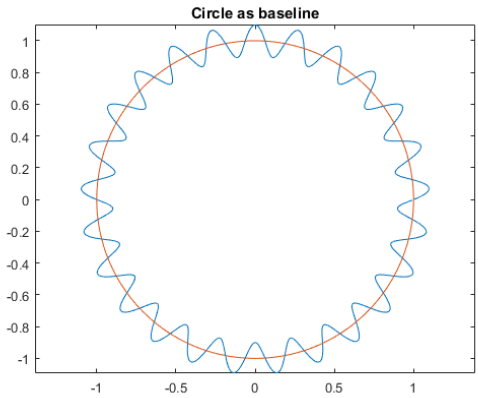

(a) Circle curve (blue) and circle baseline (red).

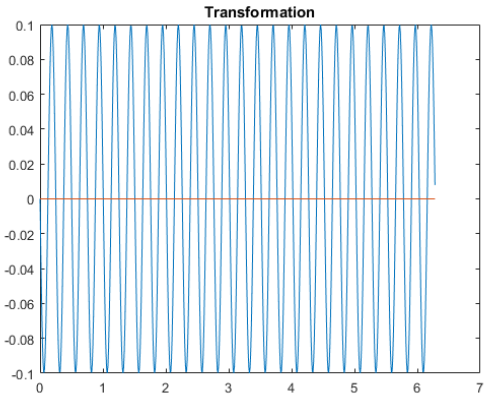

(b) Figure 10a transformation.

Figure 10: Curve and its transformation.

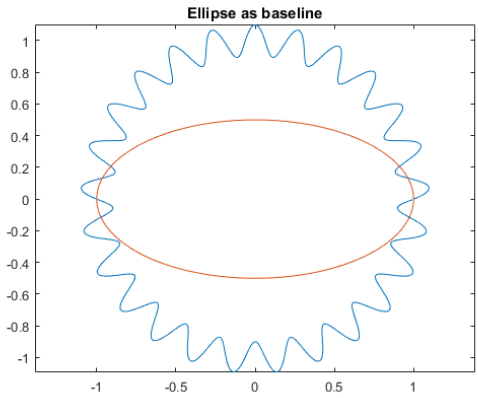

(a) Circle curve (blue) and ellipse baseline (red).

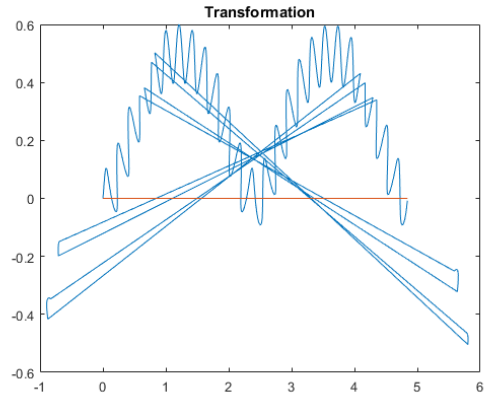

(b) Figure 11a transformation.

Figure 11: Curve and its transformation.

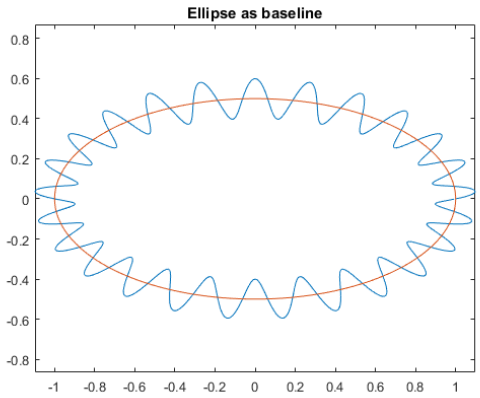

(a) Ellipse curve (blue) and ellipse baseline (red).

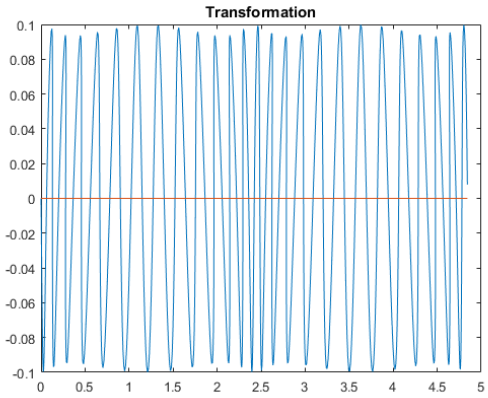

(b) Figure 12a transformation.

Figure 12: Curve and its transformation.

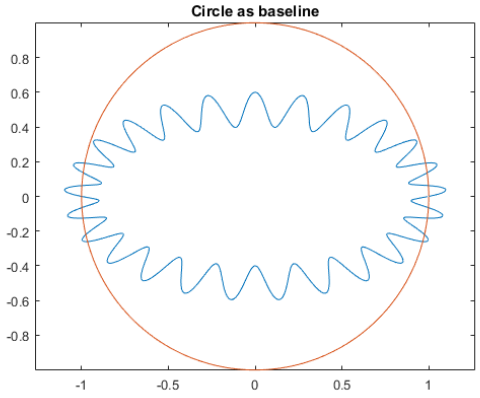

(a) Ellipse curve (blue) and circle baseline (red).

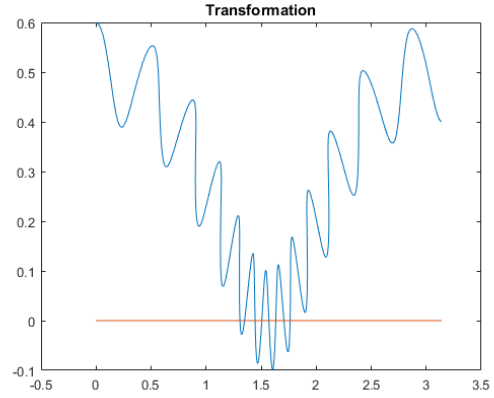

(b) Figure 13a transformation.

Figure 13: Curve and its transformation.

As it can be observed, the more accurate transformation is achieved for the baseline that has the same geometry as the sinusoidal plot, because it shows the configuration expected after the transformation that in this case is the sinusoidal distribution. It can be concluded that the baseline needed to perform the analysis must fit the shape of the profile obtained from the data to be processed.

In addition, looking at figure 13b the appearance of some disturbances are detected after the transformation is performed. Changing the shape of the baseline, in this case the radius of the ellipse, it is noticed that the variation of the parameters of the curve affect the conversion result as shown in figure 14 and figure 15.

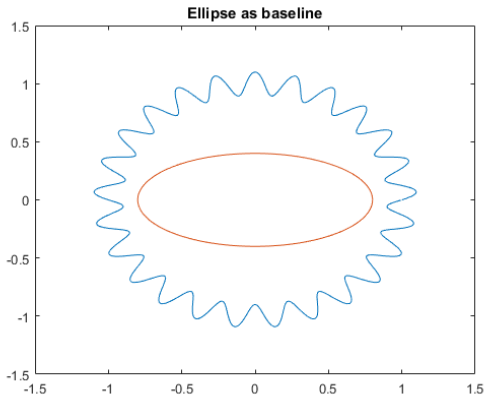

(a) Circle curve (blue) and ellipse baseline (red).

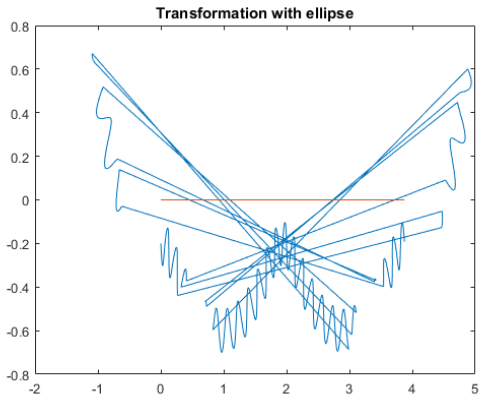

(b) Figure 14a transformation.

Figure 14: Curve and its transformation with reduction of radius.

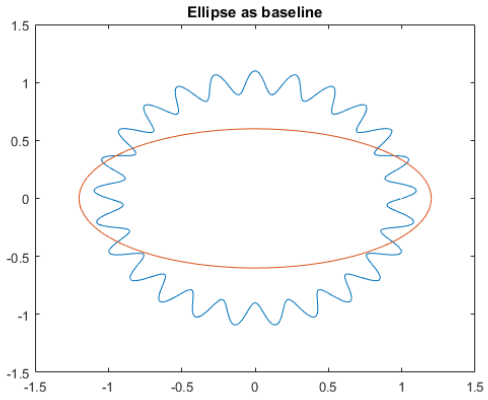

(a) Circle curve (blue) and ellipse baseline (red).

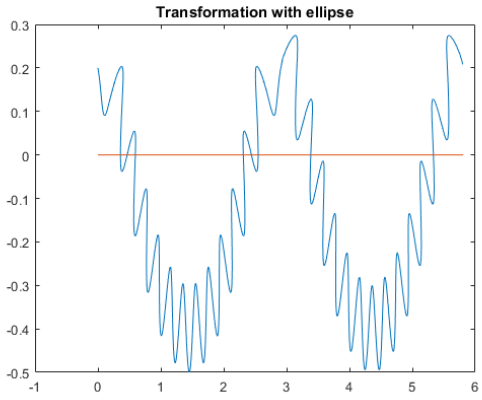

(b) Figure 15a transformation.

Figure 15: Curve and its transformation with increment of radius.

The previous figures reflect that if the radius is reduced the conversion achieved is poorer, while increasing it makes the transformation be more favorable, but it

is not as decent as the ones in which the geometry of the baseline coincides with the parametric curve shape.

4.3 Geometrical shape

By the representation of the considered profiles given in figure 5, it can be observed that they seem to be similar to half of the geometries given in 2.2; the shapes that are going to be analyzed are a semi-circle, a semi-ellipse and also a parabola. The semi-circle and semi-ellipse are defined by equations 3 and 4 respectively changing the parameter t to be from $-\frac{\pi}{2}$ to $\frac{\pi}{2}$ radians. The parabola is established by the equation 7, where t_P is a set of values that goes from -2π to 2π radians. This new academic characterization are represented in figure 16.

$$\begin{aligned} x &= t_p^2 \\ y &= t_p \cdot (R + A \cdot \sin(n \cdot t)) \end{aligned} \tag{7}$$

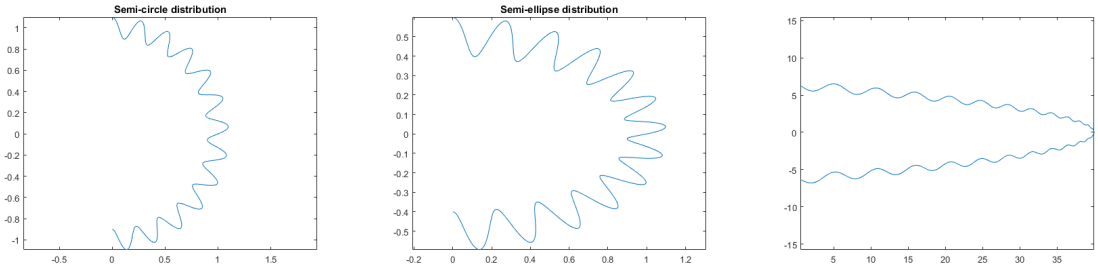

(a) Semi-circle profile. (b) Semi-ellipse profile. (c) Parabola profile.

Figure 16: Half of geometry profiles.

As explained in Section 4.2, the baseline must be selected for each one of the geometries: As it was proved before, the baselines represented in figure 17a, figure 18a and figure 19a are the ones that fits in an appropriate way for each curve, they are shown in red color. For the profiles, the baselines are defined varying the parameter t to be from $-\frac{\pi}{2}$ to $\frac{\pi}{2}$ radians, except for the parabola that is specified in equation 8. Once the baseline is defined, then the transformation of coordinates is implemented obtaining the results shown in figure 17b, figure 18b and figure 19b.

$$x = t_p^2$$
$$y = t_p \tag{8}$$

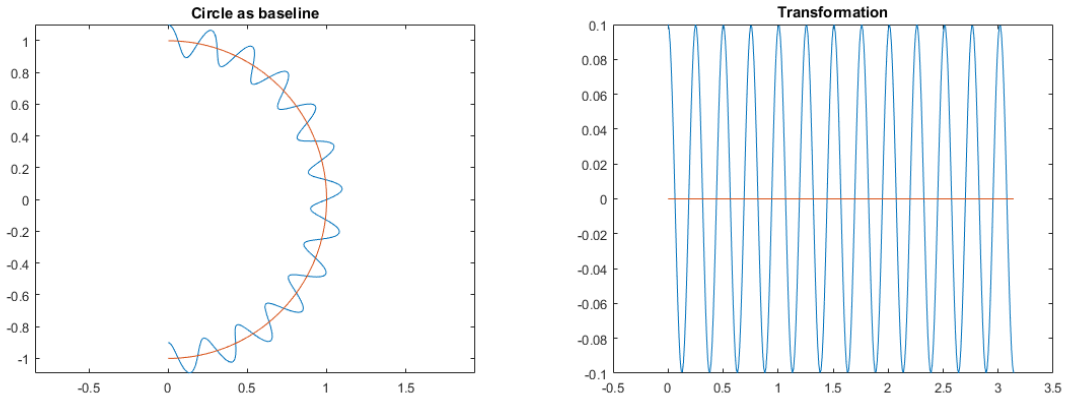

(a) Semi-circle (blue) with its baseline (red).

(b) Transformation with semi-circle.

Figure 17: Semi-circle.

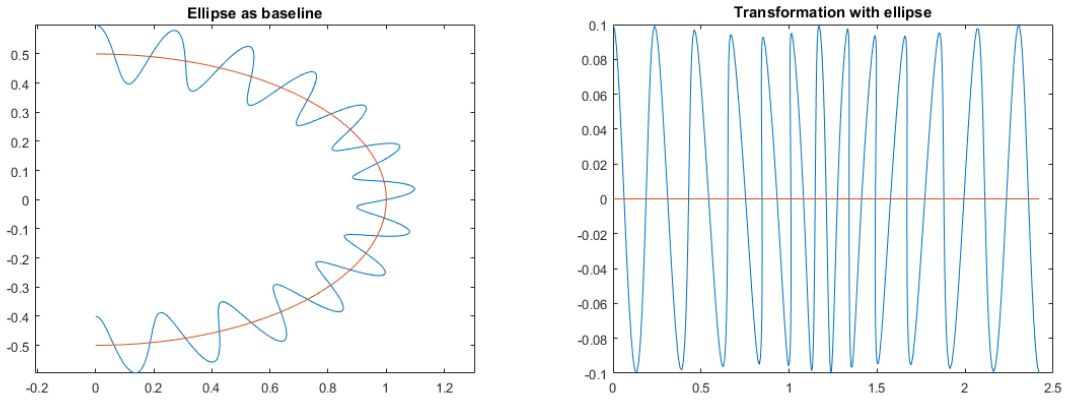

(a) Semi-ellipse (blue) with its baseline (red).

(b) Transformation with semi-ellipse.

Figure 18: Semi-ellipse.

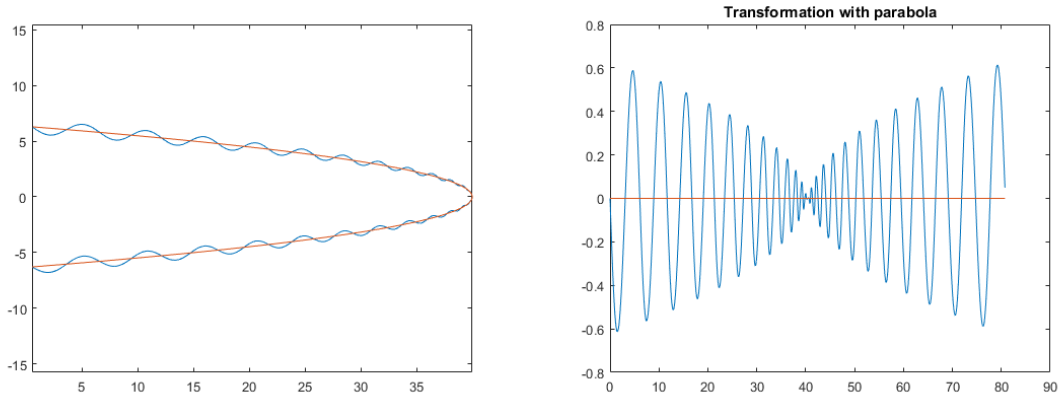

(a) Parabola (blue) with its baseline (red).

(b) Transformation with parabola

Figure 19: Parabola.

Comparing the prescribed profiles with the transformed ones illustrated in figure 17, figure 18 and figure 19, it can be detected that the transformation is performed properly as it represents all the points characterized in the academic curves as expected in the new illustration. The horizontal red line is the conversion related to the baseline and it represents the length of its profile.

In figure 19, the process for the parabola is depicted, however in contrast to the geometries of semi-circle and semi-ellipse, the original geometry had a varying sinusoidal pattern which decreased its amplitude as the parabola approached its peak. This is reflected after the transformation with a pattern that had a curved-shaped decrease of the amplitude. However, it only proves that the method works as well as for the other examples, as the final result is the expected one.

In conclusion, the number of peaks of each profile can be counted in a simpler way looking at the plot of the converted curves. Giving appropriate representation as expected.

This process applied using the academic examples is now adapted to be used in the experimental data as it will be explained in Section 5.

5 Experimental data analysis

Once the results obtained from the theoretical curves are adequate, the procedure can be implemented for the real data obtained. To apply the analysis, a set of images were received by experiments done at Universidad Carlos III de Madrid, as explained in Section 3.

The code developed gives as outputs the images shown in this section, but it needs certain inputs to work:

- The set of images received from the experiments.
- The code will ask for the number of the first image and the number of the last one that point the limits of the range in which the code will operate. In this case the input of the first image is 200 and the last image is 800.
- Also, it will require to determine the interval inside the range of the images selected previously. This step is important to appreciate a significant difference between images. For this analysis the interval selected is 40 images.

These images must be converted so as to be processed using ®MatLab, due to the necessity of the software to work with matrices. In order to transform the data into matrices, the function used is *imread* that reads the image from a graphics file. The result can be observed in figure 20. The next step is to binarize it, since the objective is to extract the perimeter because the function utilized to derive the contour works with binary data. To do this conversion, the necessary function is *imbinarize*, obtaining the image represented in the figure 21. All the results illustrated in this section belong to the image number 560 of the whole data.

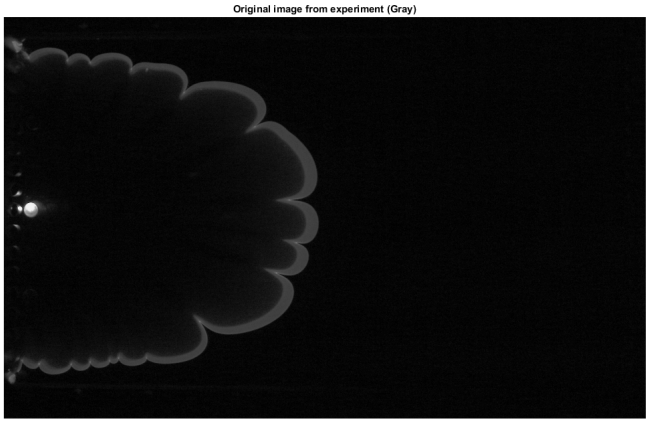

Figure 20: Real Image.

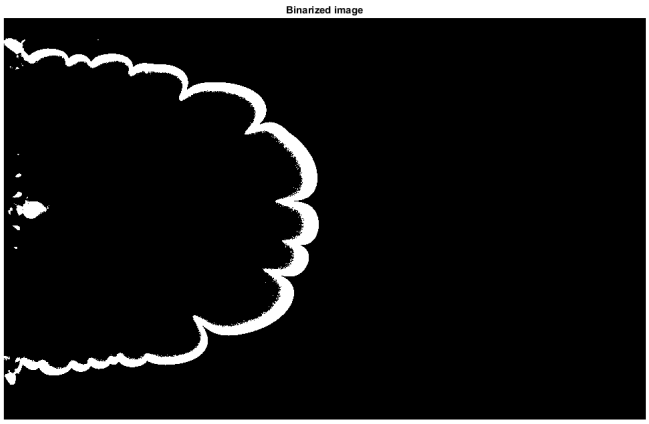

Figure 21: Binarized Image.

Depending on the image received from the experiment, it may be necessary to make another extra conversion as the image must be in grayscale to apply the binary conversion. If it is not, the function *rgb2gray* converts an RGB image or colormap to grayscale.

After being able to binarize the data, the principal aim is to find a way to extract the boundary of the flame. This process can be achieved using *bwboundaries*

that gives a set of cells, each one containing all the boundaries of the objects inside the image. As the objective is to find the one that belongs to the flame, a process to determine this perimeter was developed, it consists on selecting the cell that has the greater number of points, obtaining the contour shown in the figure 22. The most interesting disturbances are the ones located at the outer contour of the flame, therefore, the inner perimeter was removed as represented in figure 23 to discard the profiles that can obstruct the proper study of these instabilities.

Also, the values of the profile close to the limit of the Hele-Shaw cell were eliminated due to the noise appearing in that location as noticed in figure 5.

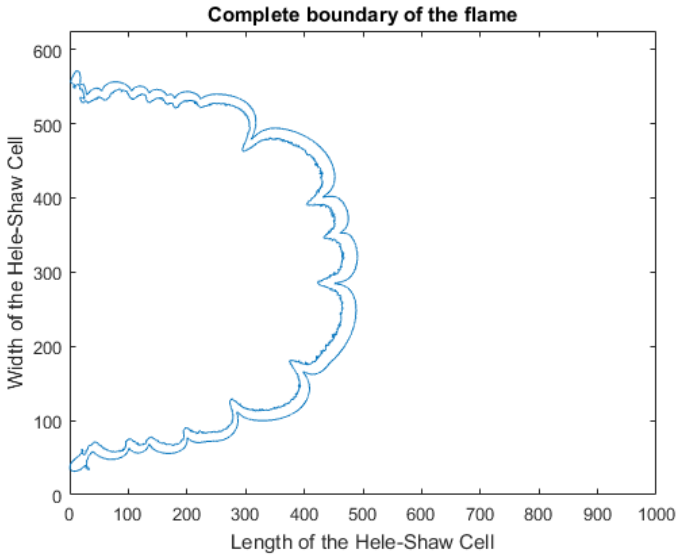

Figure 22: Whole contour of the flame.

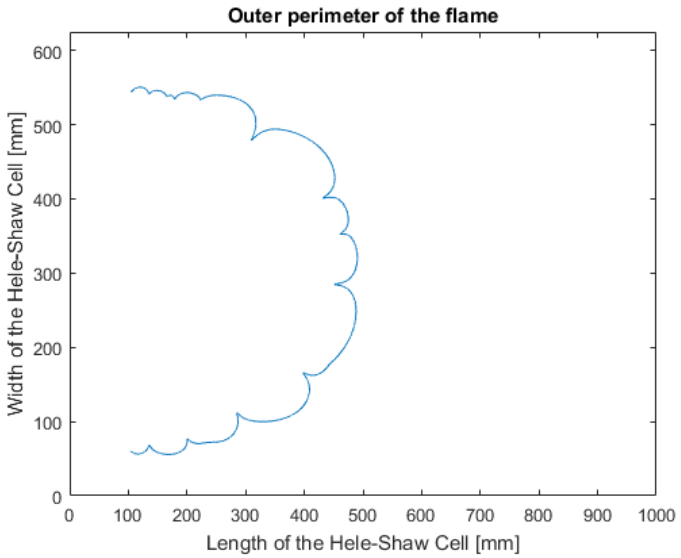

Figure 23: External perimeter.

Once the desired curve is obtained, the baseline is selected, since it is essential to make the transformation as explained in Section 4.1. In this case, the ellipse was the baseline selected due to its similarity with the profile given in figure 5 and its simplicity to operate with it. The baseline is processed and finally obtained as shown in figure 24.

In order to achieve a proper baseline, these parameters must be set:

- The x-position of the baseline's center is the point where the representation of the flame starts.
- The y-position of the baseline's center is defined by equation 9:

$$Y_c = Y_{min} + Y_{max} - \frac{Y_{min}}{2} \tag{9}$$

  Where Y_{min} and Y_{max} are the maximum and minimum y-coordinate of the representation of the flame contour.

- The length of the semi-major axis of the ellipse is the distance from the center of the geometry to the value of x of the contour that coincides with Y_c.

- The length of the semi-minor axes is half of the distance between Y_{max} and Y_{min} as seen in equation 10:

$$Y_r = \frac{Y_{max} - Y_{min}}{2} \tag{10}$$

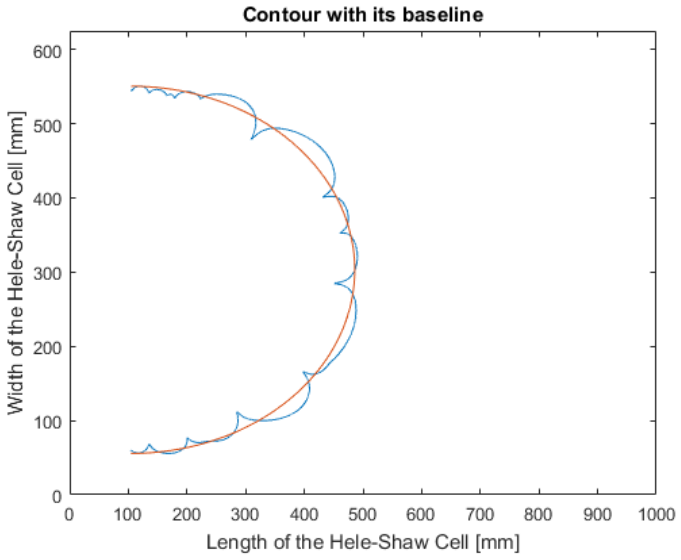

Figure 24: Contour (blue) and baseline (red).

Following the same process as in Section 4, the transformation from Cartesian to curvilinear coordinates is implemented and it gives the structure given in figure 25. Some additional methods were developed: In these procedures the main function used is *smooth*, that decrease the not desired noise found in the response data, eventually obtaining a good representation of the signal given by the exterior perimeter as shown in figure 26. Also, an inversion of the modified curve is realized to get an adequate visible form to observe the peaks. This final depiction is reproduced in the figure 27.

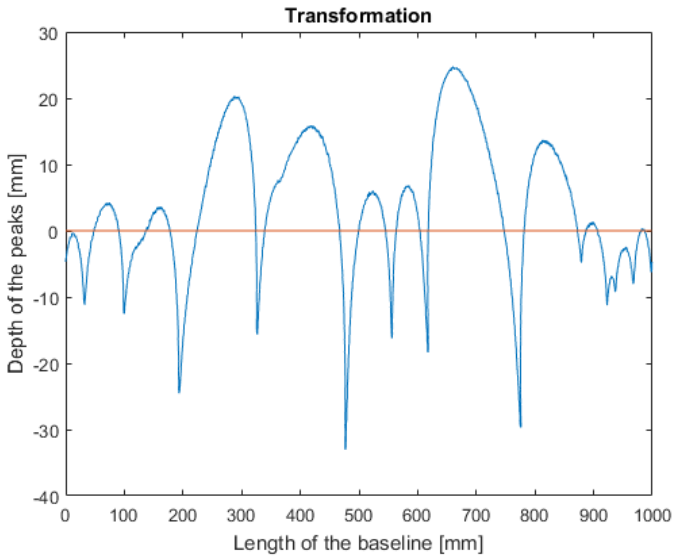

Figure 25: Transformation from Cartesian to curvilinear coordinates.

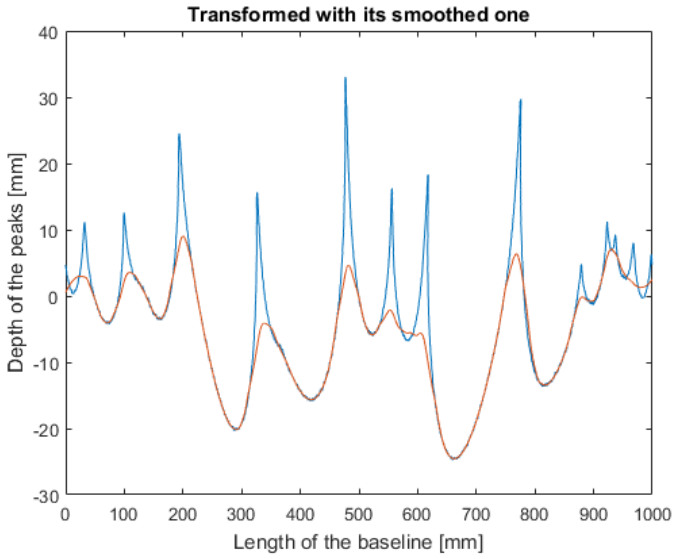

Figure 26: Transformation (blue) with its smoothed representation (red).

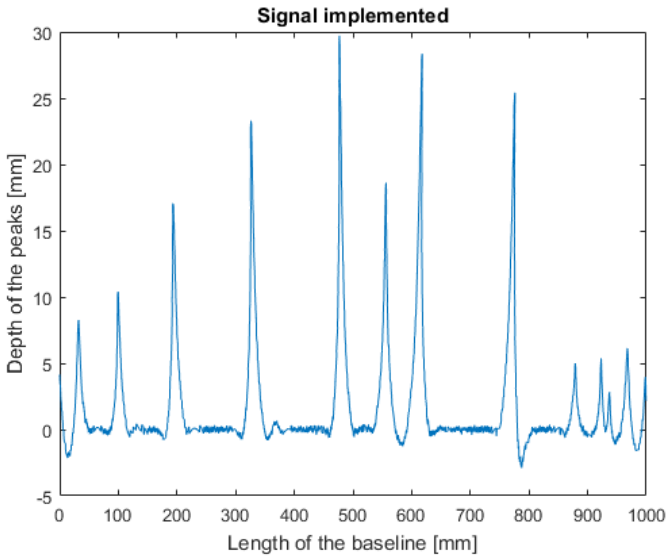

Figure 27: Signal obtained from the exterior diameter.

The final objective is to know how the number of peaks evolves through the whole number of images, as it will provide the information about the instabilities affecting the flame. Thus, it is necessary to develop a process to count the number of peaks and represent them.

First, the function *findpeaks* was implemented, however, the output received was not as expected due to the noise appeared in all the images. So, a new function called *peakfinder*, taken from [16], was carried into effect, getting better results than for the previous one. In figure 28 there is a comparison of the peaks with the original perimeter that was analyzed. It can be observed that the peaks shown in figure 28b are the same that appears in 28a, thus, this validates the process performed during the analysis.

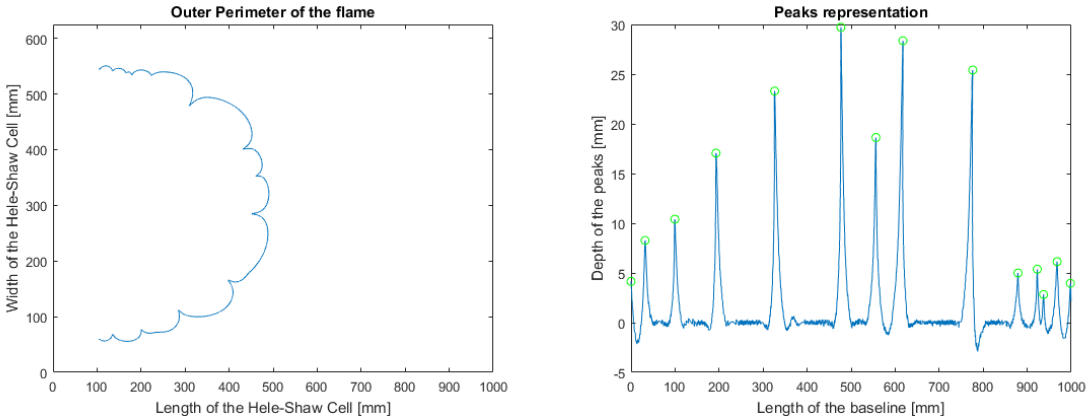

(a) Outer Perimeter. (b) Peaks.

Figure 28: Comparison between the original contour and the representation of its peaks.

A set of 16 images were selected in order to perform the whole analysis and to locate the peaks that represent the instabilities that appears at different time intervals. Figure 5 shows all 16 images together that begins from picture 200 to 800, by this way it can be appreciated how the shape of the flame changes and how the instabilities increase through time.

All the figures of the exterior contour and the peaks that belongs to the whole set of images are displayed in Appendix B where the peaks obtained can be checked comparing them with their respectively perimeter.

Finally, in the following figures it is shown the evolution of the number of peaks (figure 29) of the flame, and the length through time of the external contour given in pixels (figure 30a) and the length of the baseline given in millimeters (figure 30b) for each of the flame perimeters shown in figure 5. The time is calculated dividing the total number of images from the set of data by the value of the fps at which it was recorded.

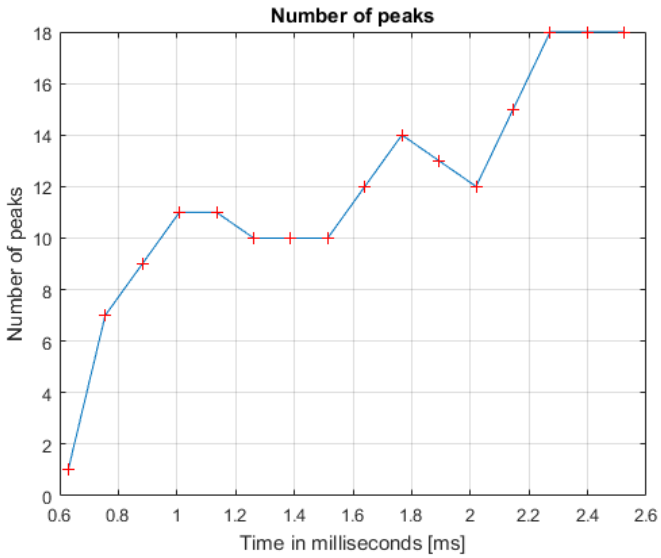

Figure 29: Number of peaks through time.

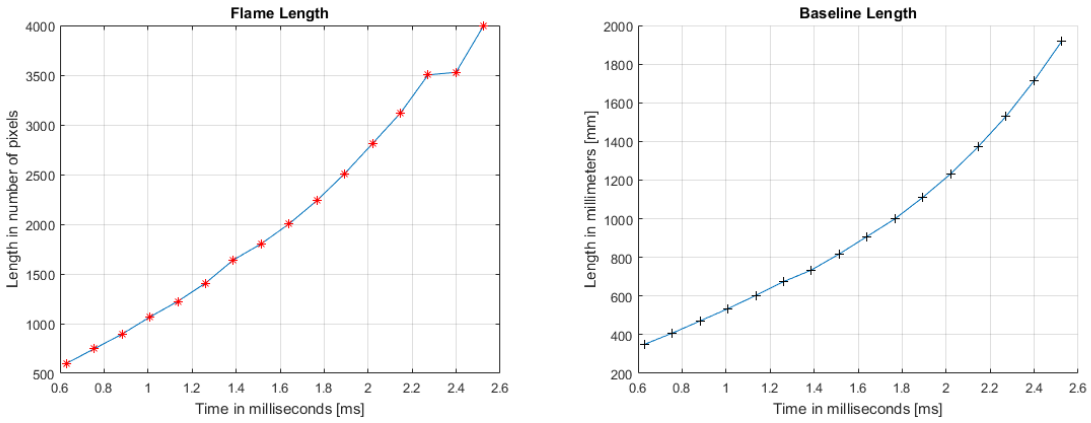

(a) Flame length in pixels.

(b) Baseline length (mm).

Figure 30: Flame and baseline length through time.

The length calculated is the value of the exterior flame's perimeter analyzed during the process. Also, the length of the baseline was computed noticing that it increases with a similar behavior than the contour, as expected.

Alternatively, the length of the flame in metric units is computed applying equation 11 , obtaining the result show in figure 31.

$$L = \int_a^b \sqrt{(1 + (\frac{dy}{dx})^2} \cdot dx \tag{11}$$

Where:

- L is the length of the curve give in millimeters.
- a and b are the first and last limits of the curve respectively.
- dy and dx are the differential of the y and x coordinates of the curve respectively.

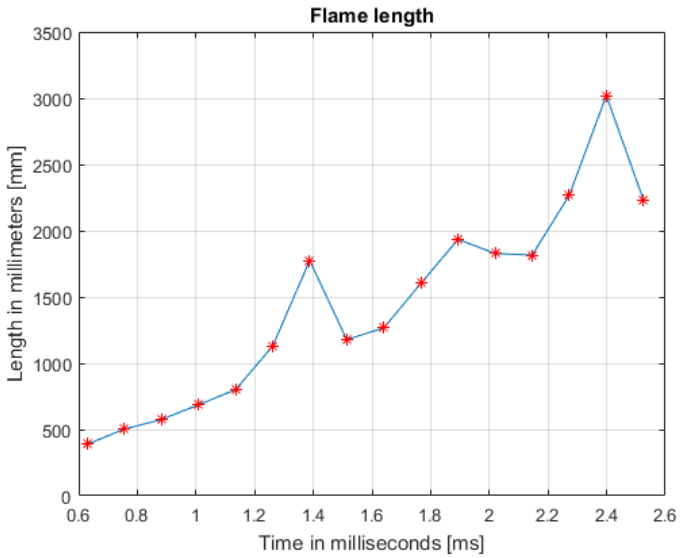

Figure 31: Length of the flame in millimeters.

It is visible that the behavior of the flame length in millimeters is the expected one as it increases during the time as seen in figure 30a, but there is an abrupt rise in the sixth image, whose contour is displayed in figure 37a and looking at it and comparing it with the next and previous one the length should have a different value than the obtained, so this issue may have happened due to some miscalculation or wrong data taken. The same occurs for the second-to-last image, whose

perimeter is shown in figure 46a.

Despite that, the number of peaks and the length of the flame, increase. However, in figure 29 there are images that have less number of peaks. This circumstance might be explained by the lack of accuracy of the function used for counting the peaks.

Lastly, the behavior of the graphs is the expected one, so it can be considered that the system employed to analyze the images is almost successful.

6 Conclusion and prospective

The main objective of the work accomplished was to develop a method to characterize the instabilities appearing in the flame front of a combustion process.

In the frame of this experiment, the device used to capture the instabilities was a High Speed Camera recording the flame propagation presented in the reproduction of the Hele-Shaw cell made at the Universidad Carlos III de Madrid laboratories.

To achieve that, some fundamental aspects must be taken into account:

- The transformation from Cartesian coordinates to channel-fitted curvilinear coordinates, since it provides a simpler recognition of the peaks that are the points of interest to identify the instabilities produced.
- The creation of academic prescribed profiles in which the method will be implemented before executing it for experimental data.
- To develop baselines for each of the profiles, since they are necessary for the transformation to be implemented. From these baselines, the most appropriate is selected and applied for the conversion.

After realizing that process, the work with the experimental data received begins, in which the method carried out for the academic profiles is reproduced. The main difference appearing in real data is that a conversion must be done to allow ®MatLab to work with the set of images.

Finally, the peaks can be easily identified for each of the images analyzed and also the way the exterior contour of the flame varies through the time. The results show that the number of peaks increases with time proving that the instabilities grow when the flame is propagating.

6.1 Prospective

Despite the image processing method implemented achieves the main objectives of the project, further tasks related to extract meaningful information may be performed:

- Applying the same method developed for the outer contour, the inner contour can be processed to track the flame interface of this perimeter and compare it with the one obtained from the exterior boundary.
- Also, to elaborate a procedure to characterize the local curvature of the cells, that is, instead of analyzing the whole flame, each cell is taken individually and then processed its instabilities.

Therefore, the image processing can be utilized in future works in order to characterize in the best way flame instability and its evolution through time.

Appendices

A Socio-economic environment

The method developed throughout this project will simplify the identification of flame instabilities making possible to point where and when they appear. So, the way to counteract these disturbances will improve.

Considering the control of the instabilities developed during this experiment, the project can generate a benefit in economic and environmental terms:

As explained in Section 1, flame instabilities are the cause of some important issues in combustion processes. From an economic perspective, the code developed could help increase the combustion engines efficiency and their life-span, which directly leads to a reduction in labor, materials, fuel and energy.

In addition, if the project is analyzed from an environmental point of view, the previously mentioned improvements have a direct effect on the reduction of the raw materials used and of the pollutant gases produced.

A.1 Project's budget

Despite the experimental process is not taking into account, since the data is freely received, the analysis requires of some devices that must be taken into account as well as the time spent by the person that implements and creates the analysis. The budget is detailed in the following table:

Item	**Price per unit**	**Units**	**Total**
®MatLab Student License	69€	1	69€
Computer Asus A73S	765€	1	765€
Worker salary	15€/h	300 hours	4500€
TOTAL			5334€

Table 1: Project Budget

B Peaks' figures

In this appendix all the figures that represent the combination of the external contour and its corresponding peaks are displayed:

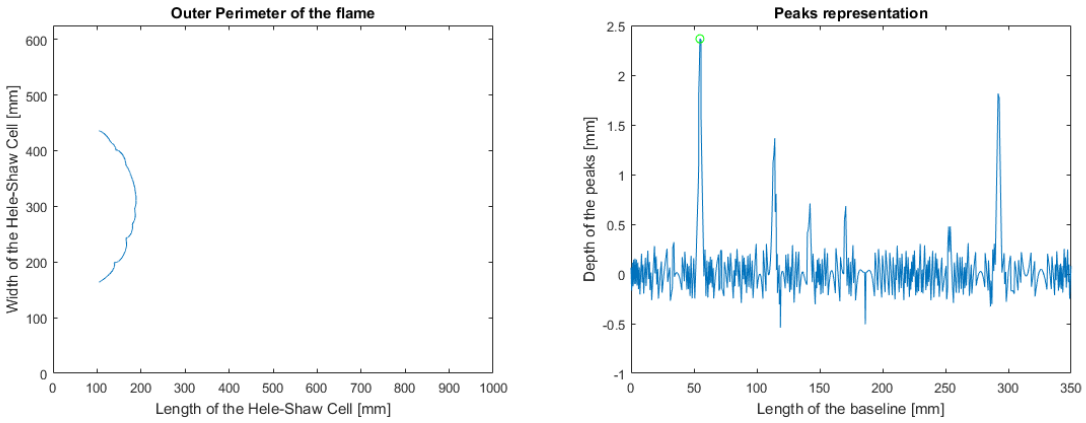

(a) Outer Perimeter. (b) Peaks.

Figure 32: Image Number 200.

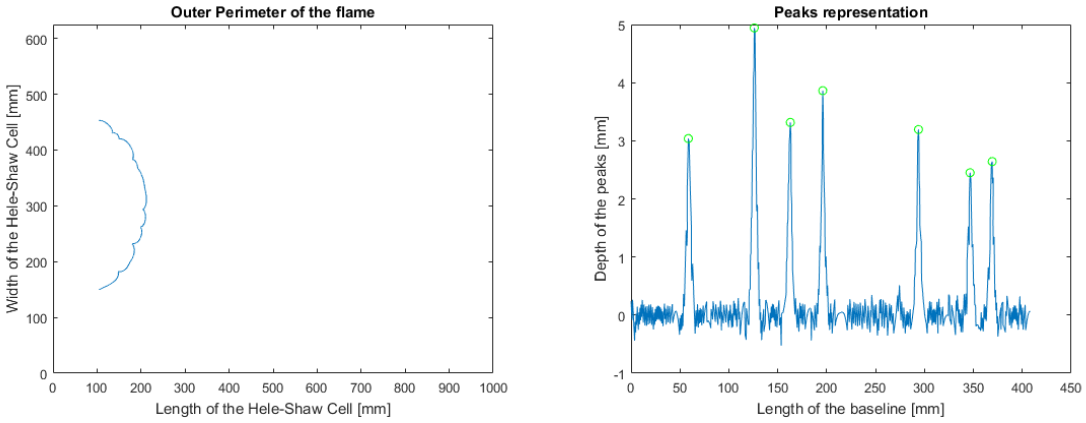

(a) Outer Perimeter. (b) Peaks.

Figure 33: Image number 240.

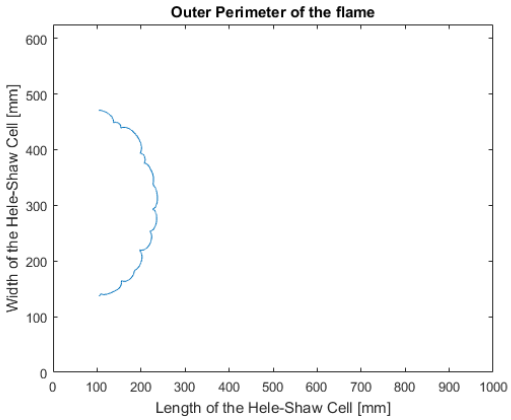

(a) Outer Perimeter.

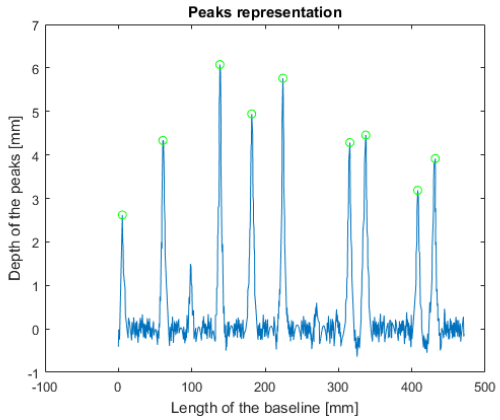

(b) Peaks.

Figure 34: Image number 280.

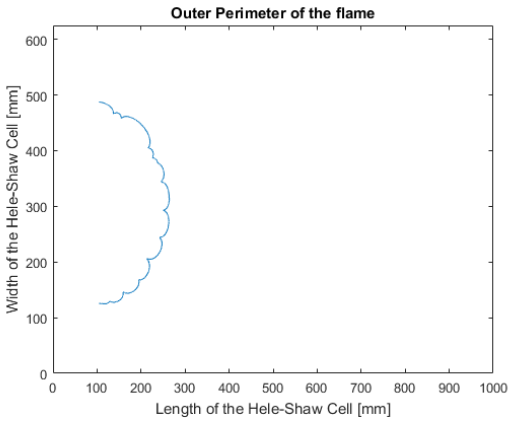

(a) Outer Perimeter.

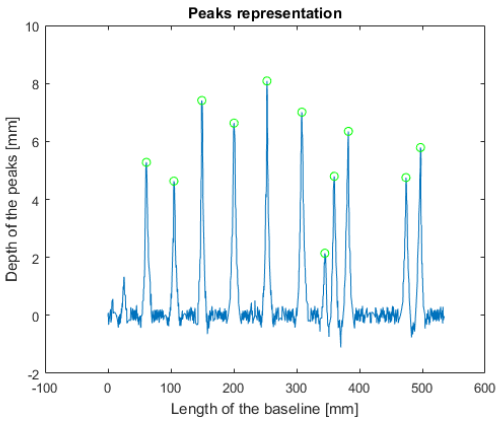

(b) Peaks.

Figure 35: Image number 320.

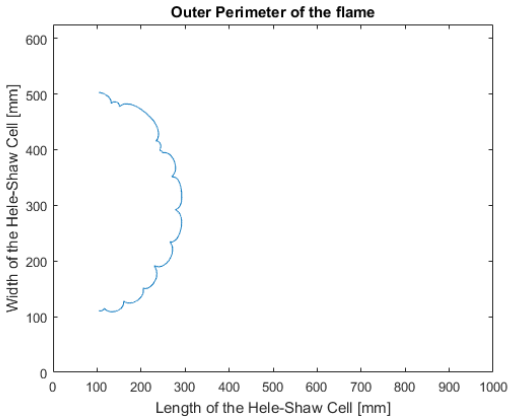

(a) Outer Perimeter.

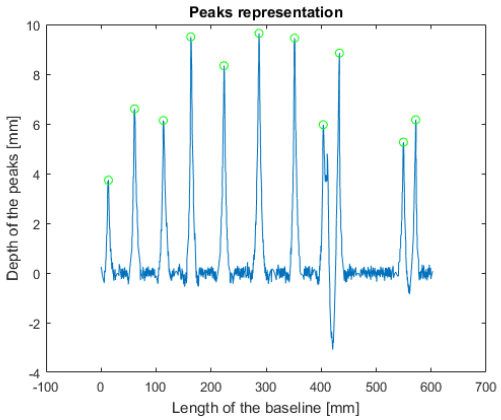

(b) Peaks.

Figure 36: Image number 360.

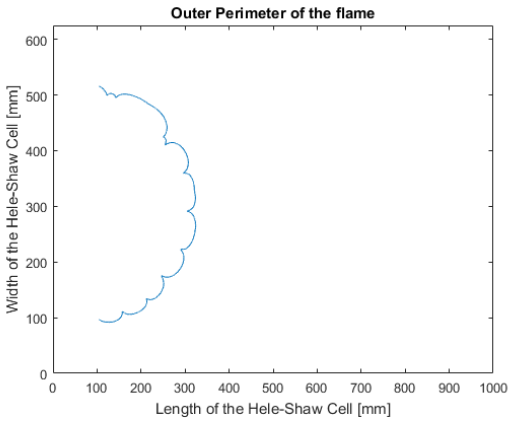

(a) Outer Perimeter.

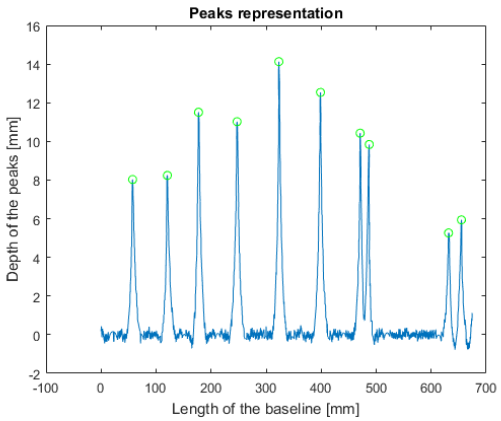

(b) Peaks.

Figure 37: Image Number 400.

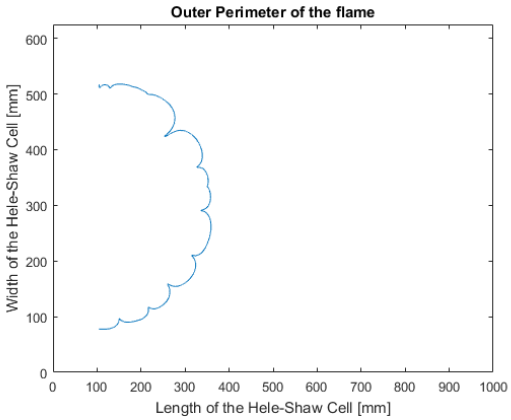

(a) Outer Perimeter.

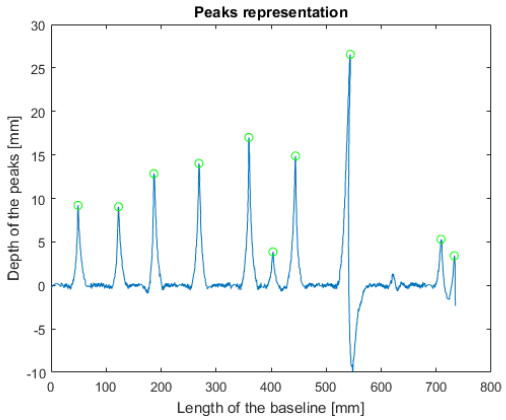

(b) Peaks.

Figure 38: Image Number 440.

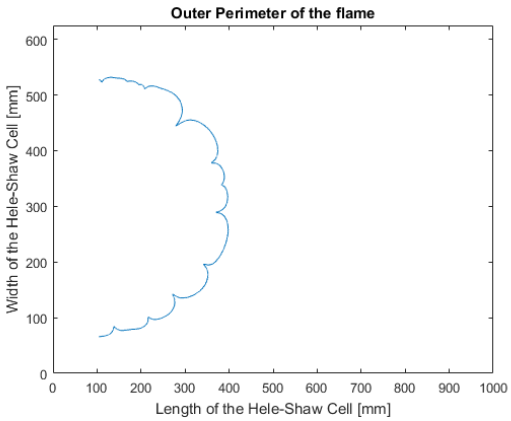

(a) Outer Perimeter.

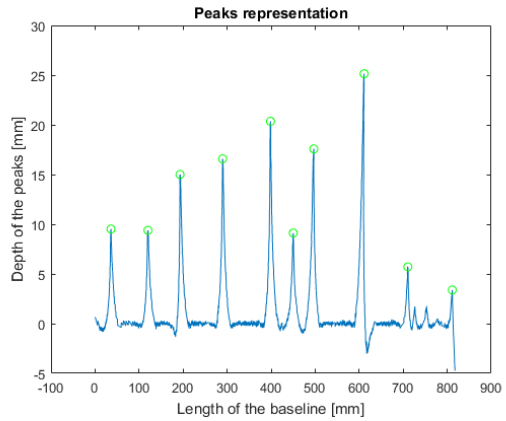

(b) Peaks.

Figure 39: Image Number 480.

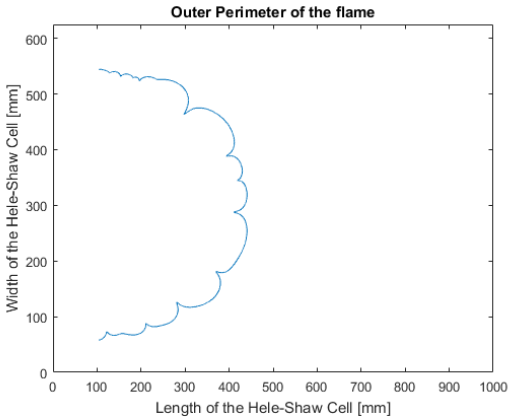

(a) Outer Perimeter.

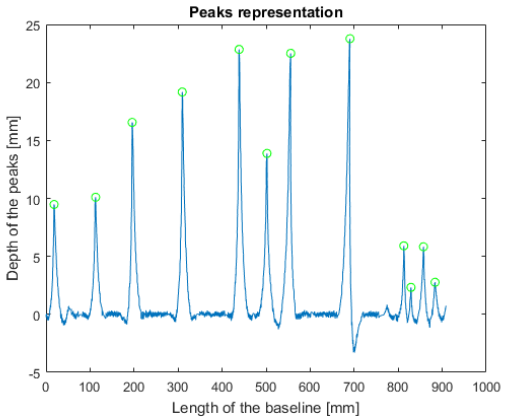

(b) Peaks.

Figure 40: Image Number 520.

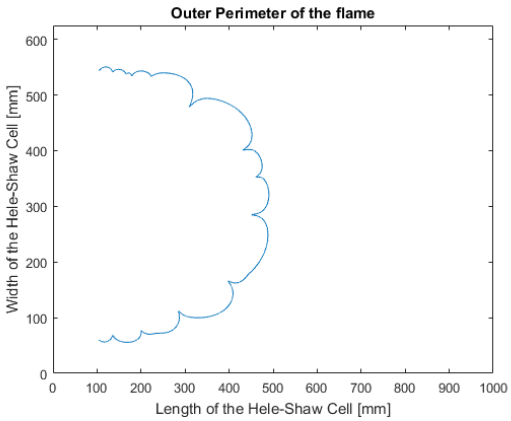

(a) Outer Perimeter.

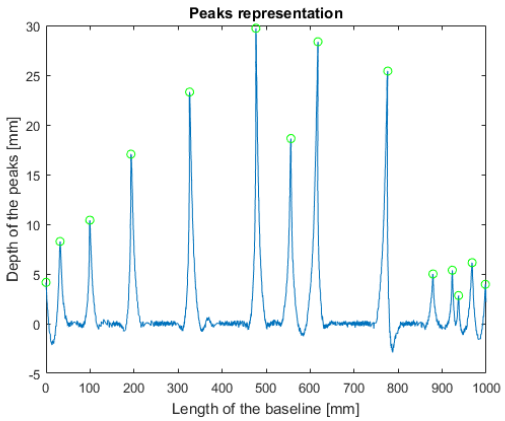

(b) Peaks.

Figure 41: Image Number 560.

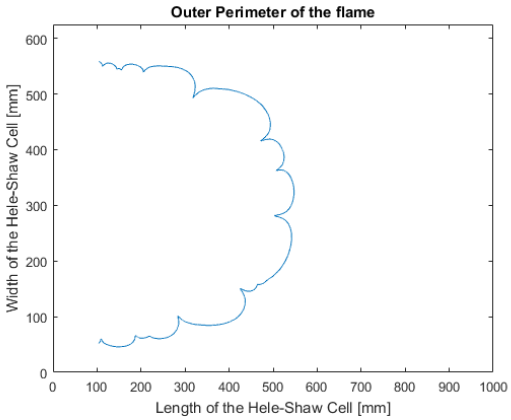

(a) Outer Perimeter.

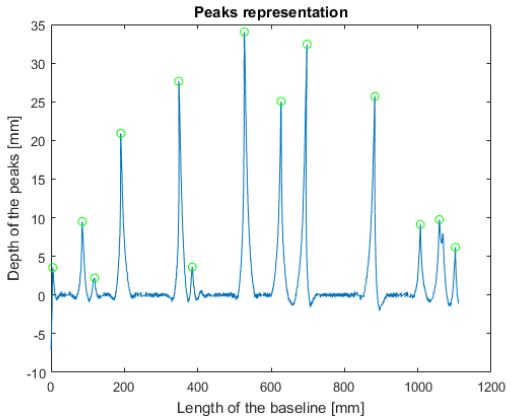

(b) Peaks.

Figure 42: Image Number 600.

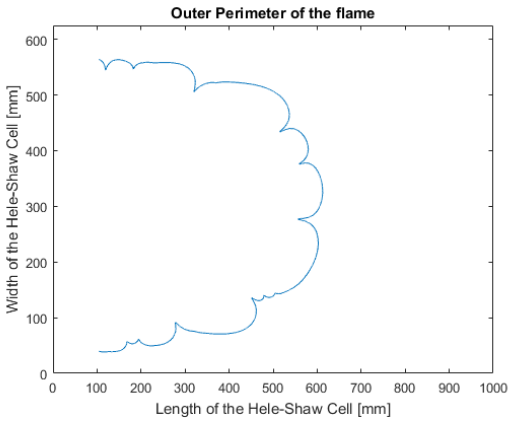

(a) Outer Perimeter.

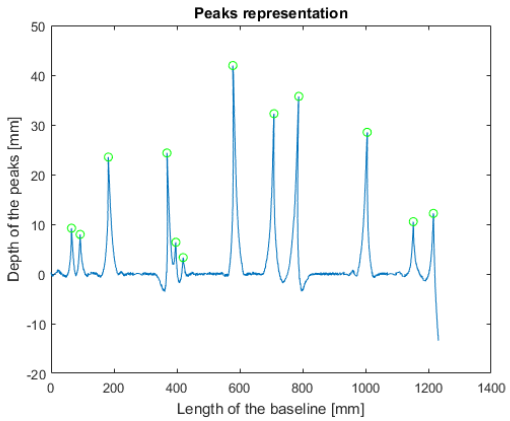

(b) Peaks

Figure 43: Image Number 640.

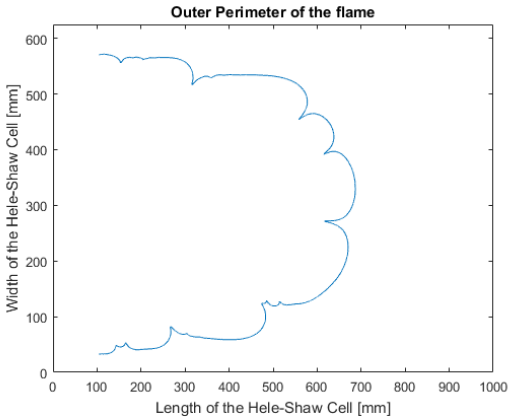

(a) Outer Perimeter.

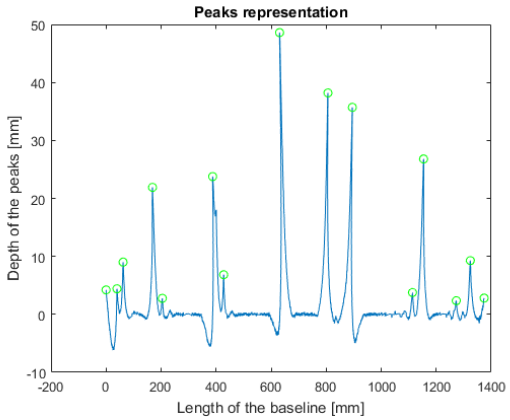

(b) Peaks.

Figure 44: Image Number 680.

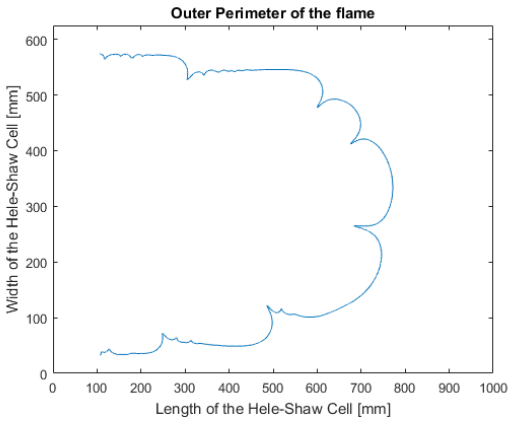

(a) Outer Perimeter.

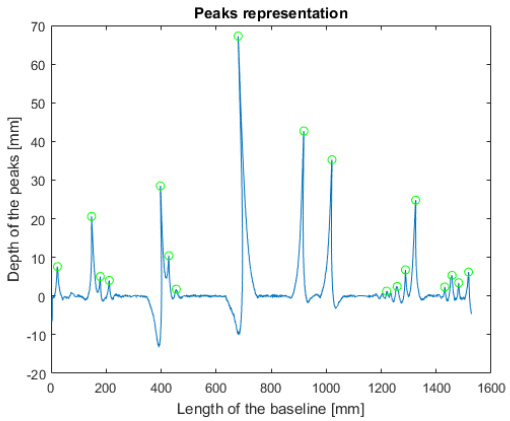

(b) Peaks.

Figure 45: Image Number 720.

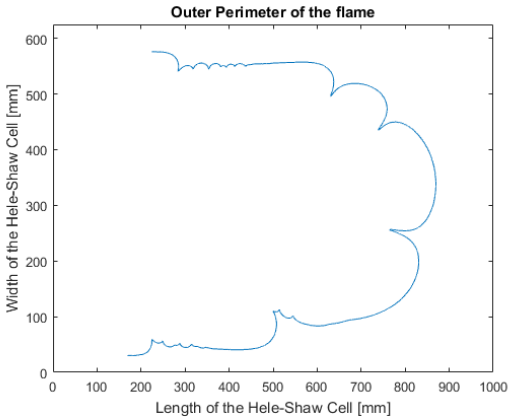

(a) Outer Perimeter.

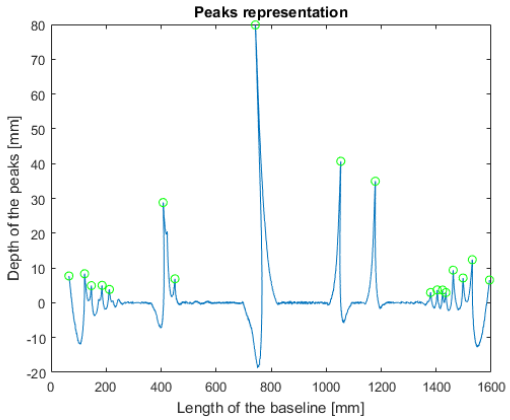

(b) Peaks.

Figure 46: Image Number 760.

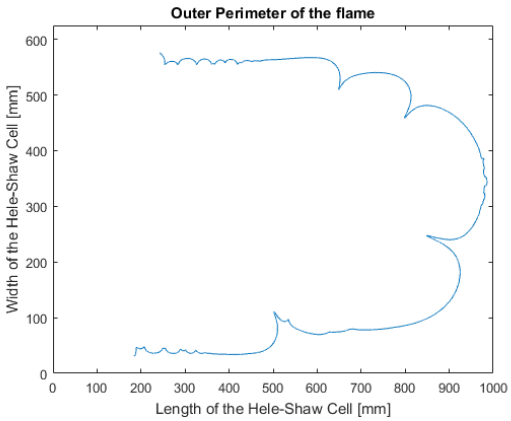

(a) Outer Perimeter.

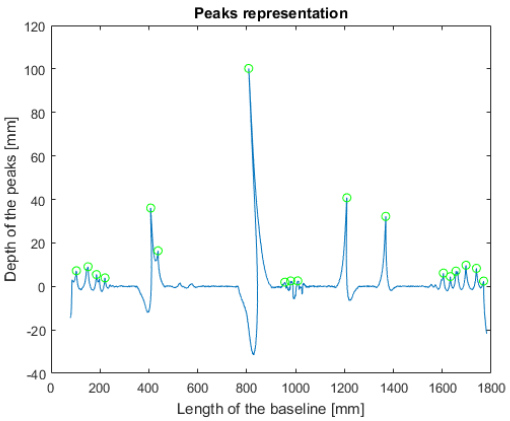

(b) Peaks

Figure 47: Image Number 800.

References

[1] Lipika Kabiraj, Aditya Saurabh, Pankaj Wahi, R. I. Sujith, *Route to chaos for combustion instability in ducted laminar premixed flames*, Department of Aerospace Engineering, Indian Institute of Technology Madras, India. Department of Mechanical Engineering, Indian Institute of Technology Kanpur, India, 22, Page 1, Published online 23 May 2012.

[2] T. H. New, et al. *Experimental Study on Deflagration-to-Detonation Transition Enhancement Methods in a PDE*, Department of Engineering, University of Liverpool, Temasek Laboratories, National University of Singapore, Aerodynamics Research Center, Mechanical and Aerospace Engineering Department, University of Texas at Arlington.

[3] V. E. Volkov, *One-dimensional flame instability and control of burning in fire-chamber*, Odessa Natinal Academy of Foood, Page 1, 2015.

[4] N. Noiray, D. Durox, T. Shuller, S. Candel, *A unified framework for nonlinear combustion instability analysis based on the flame describing function*, Cambridge University Press, Published online: 25 November 2008.

[5] C. Clanet, G. Searby, *First Experimental Study of the Darrieus-Landau Instability*, CNRS - Universités d'Aix-Marseille I & II, Campus Universitaire de St. Jérome, France, Page 1, 1997.

[6] Geoff Searby, *Experimental studies of instabilities of laminar premixed flames*, Institut de Recherche sur les Phénoménes Hors Équilibre, Université de Provence, France, International Conference on Combustion and Detonation, Zel'dovich Memorial II, Moscow, Page 2, 2004.

[7] Cepsa, *Ficha de datos de seguridad*, 2012.

[8] Official MatLab Web Page, *MatLab Student License*, https://www.mathworks.com/academia/student_version.html?s_tid=hp_ff_p_student, 2017.

[9] Daniel Fernández-Galisteo, Vadim N. Kurdyumov, Paul D. Ronney, *On the premixed flame propagation between two closely spaced parallel plates*, Department of Energy, CIEMAT, Madrid. Department of Aerospace and Mechanical Engineering, University of Southern California, Los Angeles, Pages 1-3, 2016.

[10] David P. Schmidt, *Laminar flame propagation in mixtures with compositional stratification at small length scales*, Thesis, Master of Science in Mechanical Engineering, University of Illinois, Urbana, Illinois, 2011.

[11] Moshe Matalon, *Lecture 8: Flame stretch and Lewis number effects*, 5 and 11, 2011.

[12] Brian J. Kirby, *Bounded Stokes flow*, Cornell University, College of Engineering, Kirby Research Group, Ithaca, http://www.kirbyresearch.com/textbook.

[13] Nac Image Technology, *Memrecam HX-3 Specification Sheet*, http://www.nacinc.com/datasheets/Memrecam%20HX-3%20Specification%20Sheet.pdf.

[14] Robert Bosch, *Glow Plugs*, Bosch, 2010, Retrieved 2012-07-07.

[15] Carl J. Legleiter, Phaedon C. Kyriakidis, *Forward and Inverse Transformations between Cartesian and Channel-fitted Coordinate Systems for Meanding Rivers*, Mathematical Geology, Vol. 38, No. 8, Pages 2-11, 2006.

[16] Nathanael Yoder *Peakfinder: Quickly finds local maxima or minima in a noisy signal*, http://es.mathworks.com/matlabcentral/fileexchange/25500-peakfinder-x0–sel–thresh–extrema–includeendpoints–interpolate-, Updated 02 Oct 2016.